SAND2013-10389C

Ab Initio Calculation of Unimolecular Spin-forbidden Transition Rate Coefficients in Biradical C_2H_4O

Xiaohu Li[a,*], Judit Zádor[a,**], Ahren W. Jasper[a,**]

[a] *Combustion Research Facility, Sandia National Laboratories, 7011 East Avenue, Livermore, CA 94550 U.S.A.*

Abstract

Colloquium: Reaction kinetics

Total length of the paper determined with **Method 1**: 3895

Main text: 2322

Equations: 112 (equation 1: 8; equation 2: 8; equation 3: 16; equations 4: 16; equation 5: 16: equation 6: 32; equation 7: 16;)

References: 332

Tables: 228

Figures: 901 (figure 1: 407; figure 2: 494)

*Principal corresponding author

**Corresponding author

Email addresses: xli@sandia.gov (Xiaohu Li), jzador@sandia.gov (Judit Zádor), ajasper@sandia.gov (Ahren W. Jasper)

Abstract

We investigate the unimolecular spin-forbidden transitions in the triplet biradical complex C_2H_4O formed during the C_2H_4 + O(^{3}P) reaction. A four-state(^{3}A$''$, ^{3}A$'$, ^{1}A$'$ and ^{1}A$''$) description of the potential energy surface(PES) and spin-orbit coupling(SOC) that govern spin-forbidden transitions is probed using multi-reference electronic structure methods, namely the complete active space self-consistent field(CASSCF) method and the internally contracted multi-reference perturbation theory, n-electron valence state perturbation theory(NEVPT2). The unimolecular spin-forbidden transition rate coefficient is calculated using a non-adiabatic statistical model. Two important singlet/triplet minimum energy crossing points (MECP) are located. The micro-canonical and canonical transition non-adiabatic unimolecular rate coefficient show state-specific energy and temperature-dependenent features, which may have important implications on the the branching ratios of similar reactions involving polycyclic aromatic hydrocarbons(PAH) formation.

keyword spin-forbidden non-adiabatic multi-reference transition state theory

1. Introduction

While most elementary reactions during combustion take place on a single electronic surface, some key reactions require considering multiple surfaces. A typical example is the reactions of ground state atomic oxygen, O(^{3}P), with unsaturated hydrocarbons [1, 2, 3, 4, 5, 6]. In one of the simplest of these reactions, O(^{3}P) + ethene (C_2H_4), several bimolecular channels have been observed, and intersystem crossing (ISC) to the singlet product channels accounts for ∼50% of the total flux to the various products. This reaction has been studied both experimentally and theoretically, with fairly good agreement in the branching fractions obtained from the two approaches. A key limitation of most theoretical studies of spin-forbidden reactions is the lack of validated and applicable methods for predicting the rate of ISC. In many kinetics calculations, the ISC rate coefficient is simply adjusted empirically[1]. The ISC has also been calculated using surface hopping trajectories, and branching ratios were obtained that are consistent with those from molecular beam studies[3, 6]. Surface hopping is limited as a general approach, since it requires a computationally expensive full-dimensional PESs. Existing studies have either used direct dynamics[3], where the large number of PES evaluations limits the level of electronic structure method for the PES or fitted analytic PES[6], which demands computationally intensive electronic structure calculations.

Here, we consider the use of statistical non-adiabatic methods, which require characterization of much less of the PESs and their SOC surfaces. This method may be more readily applied to analogous reactions involving larger systems, such as the reaction of O with PAHs. Specifically, we provide a study of the spin-forbidden transition in the biradical C_2H_4O that serves as a prototype of spin-changing reactions in unsaturated hydrocarbons. Both the PES and SOC are explored by two multi-reference electronic structure methods: CASSCF and multi-reference perturbation theory NEVPT2[7]. The MECPs on the singlet/triplet crossing seams are also located. A statistical formulation for the non-adiabatic unimolecular reactions [8, 9] is utilized to calculate the micro-canonical and canonical spin-forbidden transition rate coefficients. This manuscript is organized as follows: in Section 2.1, we present a four-state picture of the PES and SOC obtained from multi-reference calculations. The properties of the located MECPs are also discussed. Subsequently, the micro-canonical and canonical rate coefficients for the spin-forbidden transition are presented in Section 2.2. Finally, we conclude in Section 3.

2. Results

2.1. A four-state representation of the coupled PESs

Since we are interested in the ISC in the C_2H_4O biradical, the regions of the coupled PESs that are relevant to the ISC are investigated. There has been extensive studies on the full PES that includes the

lowest singlet and lowest triplet in this system [1, 6, 10]. This work, however, represents the first study, to our knowledge, to include the four states, namely, $^3A''$, $^3A'$, $^1A'$ and $^1A''$, using consistent multi-reference methods. The state labels are for geometries with C_s symmetry when the O atom approaches the ethene. Symmetry-broken solutions are also discussed below. The active space includes the two p orbitals from the oxygen, the C-C σ and σ^* orbitals, the C-C π and π^* orbitals, comprised of a (6,6) space. The symmetry of the CASSCF wave-functions is determined by whether one of the two oxygen p orbitals is symmetric(A') or anti-symmetric(A'') with respect to the reflection plane. The SOC is calculated using a (7,8) state-averaged CASSCF which covers all three oxygen p orbitals. The aug-cc-PVTZ [11]basis set was used for all the calculations. All calculations were carried out using the electronic structure suite program ORCA with version number 3.0.0[12].

In Figure 1(a), we present the minimum energy path(MEP) of oxygen approaching ethene at electronic state $^3A''$ and $^3A'$. The geometries on these MEPs were obtained by performing a relaxed scan(with C_s symmetry) using CASSCF and the energy was calculated with the NEVPT2 theory. The barriers for the $^3A''$ and $^3A'$ MEPs are determined to be 4.0 and 4.6 kcal/mol respectively. These barriers are higher than the 1.9 and 2.6 kcal/mol values obtained by averaging the G2M, CBS-QB3 and G3 results[1]. The 4.0 kcal/mol $^3A''$ barrier, is in good agreement with the 3.3 kcal/mol value, where the PES was fitted based on CCSD(T)/cc-pVTZ calculations[6] and 3.0 kcal/mol using multi-reference perturbation theory[10], where in both of these studies only the lowest triplet barrier was calculated. The minimum on the $^3A''$ MEP, at a CO distance of 1.43 Å(leftmost in Figure 1(a)), with energy of -22.2 kcal/mol below the C_2H_4 + O reactant, is a not fully relaxed with respect to the symmetry-breaking OCCH dihedral angle. On the contrary, the minimum for the $^3A'$ is a stationary point that lies -21.6 kcal/mol below the reactant. This value is lower than the -18.3 kcal/mol computed as the average of the methods in Ref. [1].

The broken-symmetry stationary point, arising from relaxing the OCCH dihedral angle of the $^3A''$ minimum results in a ^3A stationary point, lying -22.7 kcal/mol below the reactant. This energy is somewhat higher than the -24.0 kcal/mol value calculated using the average of methods[1] and -21.5 kcal/mol using the fitted analytic PES [6], but is significantly lower than the 18.1kcal/mol value using multi-reference perturbation theory[10]. We also note that in our (6,6) CASSCF and NEVPT2 calculations, by twisting the OCCH dihedral angle, the $^3A''$ and $^3A'$ become degenerate and converge to the ^3A state.

To see the importance of including the four states in our study, we provide a PES of all four states calculated at the $^3A''$ MEP geometries in Figure 1(b). As the oxygen approaches ethylene, the initially well-separated singlets and triplets(with a asymptotic gap of 45.3 kcal/mol, equal to the singlet-triplet gap

of atomic oxygen, see the inset in Figure 1(b)) become densely populated when the biradical is formed. The four states are within 4.3 kcal/mol relative to each other near this region.

Using the stationary geometries of the ^{3}A and ^{3}A$'$ states, we utilize the algorithms well-documented in the literature [13, 14] and implemented in the ORCA suite of programs, to locate two MECPs between the two pairs of states that have significant SOC. The algorithm directly minimizes the effective gradient[14],

$$\mathbf{g} = 2(E_1 - E_2)\mathbf{x}_1 + \frac{\partial E_1}{\partial \mathbf{q}} - \frac{\partial E_1}{\partial \mathbf{q}} \cdot \frac{\mathbf{x_1}}{|\mathbf{x_1}|}, \tag{1}$$

where $\mathbf{x}_1 = \frac{\partial E_1}{\partial \mathbf{q}} - \frac{\partial E_2}{\partial \mathbf{q}}$ is the gradient difference vector between the two surfaces. This vector is also orthogonal to the seam of crossing, thus, it is the reaction coordinate in the statistical formulation of the unimolecular non-adiabatic reactions[8].

Some of the key geometrical and energetic properties of the two MECPs are summarized in Table 1. It is clear from Table 1 that the first MECP, denoted as MECP 1, is fairly close to the ^{3}A stationary point of the biradical. On the other hand, the MECP between the ^{3}A$'$ and ^{1}A$''$ states is significantly different from the stationary point of the biradical with ^{3}A$'$ symmetry. This key difference in geometry will affect the non-adiabatic transition as will be presented in Section 2.2. We note that the SOC is calculated using the Breit-Pauli Hamiltonian and is calculated as,

$$\epsilon = |\langle \Phi^1 | \hat{H}_{\mathrm{SOC}} | \Phi^3 \rangle|, \tag{2}$$

where $\hat{H}_{\mathrm{SOC}}$ is the Breit-Pauli Hamiltonian. At both MECPs, the $\sim$60 cm^{-1} SOC is comparable to those found in the reaction O(^{3}P) + CO[15] and the CO addition to Fe(CO)$_4$[9].

2.2. Non-adiabatic spin-forbidden transition calculated using a statistical transition state theory

The non-adiabatic effects in this system are rather complex due to the number of states included. These effects include the non-adiabatic transition between the states with the same spin that is induced by either the non-adiabatic coupling term or SOC and the ISC between different spin states. We consider the SOC induced ISC as the primary non-adiabatic effect here. Furthermore, we make the assumption that the two different MECPs are independent from each other due the different symmetries the wave-functions possess.

We summarize the basic equations for the statistical formulation for the non-adiabatic unimolecular reactions as outlined in [8, 9]. The micro-canonical rate coefficient k(E) of a spin-forbidden reaction is given as,

$$k(E) = \frac{N_{\mathrm{MECP}}(E)}{h\rho(E)}, \tag{3}$$

where $N_{\mathrm{MECP}}(E)$ is the effective number of states at the MECP and $\rho(E)$ is the ro-vibrational density of states for the stationary points of the biradical C_2H_4O(^{3}A and ^{3}A$'$ in this study). The effective number of states at the MECP is,

$$N_{\mathrm{MECP}}(E) = \int_0^\infty dE_r \rho_{vr}^{\mathrm{MECP}}(E - E_r) p_{hop}(E_r), \tag{4}$$

where the $\rho_{vr}^{\mathrm{MECP}}(E - E_r)$, $p_{hop}(E_r)$ and E_r are the ro-vibrational density of states at the MECP, the double passage diabatic hopping probability at the MECP and the energy in the reaction coordinate–the coordinate orthogonal to the seam of crossing, $\mathbf{x_1}$ in Equation 1. We have computed the diabatic hopping probability based on Landau-Zener formula[16] and that derived from the weak coupling limit[17]. The Landau-Zener double passage hopping probability is defined as,

$$\begin{aligned} p_{hop}^{LZ} &= (1 - P_{LZ})(1 + P_{LZ}),, \\ P_{LZ} &= \exp\left(\frac{-\epsilon^2}{\hbar|\mathbf{x_1}|}\sqrt{\frac{\mu}{2E}}\right), \end{aligned} \tag{5}$$

where ϵ is the SOC, μ is the reduced mass along the direction of $\mathbf{x_1}$, the reaction coordinate in the spin-forbidden transition reaction. In the limit of zero velocity, the single passage diabatic Landau-Zener hopping probability $(1 - P_{LZ})$ approaches unity, which does not apply to curve crossing when the two curves are only weakly coupled. As the SOC ϵ approaches zero, the diabatic hopping probability should leads to zero as ϵ^2. Thus, Delos[17] derived a formula for the transition probability as,

$$p_{hop}^{weak} = 4\pi^2\epsilon^2 \left(\frac{2\mu}{h^2 F|\mathbf{x_1}|}\right)^{\frac{2}{3}} Ai\left[-E\left(\frac{2\mu|\mathbf{x_1}|^2}{h^2F^4}\right)^{\frac{1}{3}}\right], \tag{6}$$

where F is the geometric mean of the magnitude of the gradients from the singlet and triplet surfaces at the MECP, Ai is the airy function. In the limit of $\epsilon \to 0$, this hopping probability is finite, thus recovering the correct physics near the low energy regime.

Finally, the canonical rate coefficient is calculated according to,

$$k(T) = \frac{e^{-\frac{E_a}{kT}}}{hQ_R(T)} \int_0^\infty dE N_{\mathrm{MECP}}(E) e^{-\frac{E}{kT}}, \tag{7}$$

where $Q_R(T)$ is the canonical partition function for the stationary point of the biradical and E_a is the zero point energy(ZPE) corrected activation barrier.

All results are presented in Figure 2. We first note that results obtained using the Landau-Zener and weak coupling formulae give fairly consistent results in general. One exception is the canonical rate constant calculated using the MECP 2 between the ^{3}A$'$ and ^{1}A$''$ states, where the rate constant calculated

using Landau-Zener formula is two times that using weak coupling at temperature T $< 500K$.

In Figure 2(a), the effective number of states $N_{\mathrm{MECP}}(E)$ in Equation 4 at the two MECPs are provided. We note that this quantity at the MECP 2 is generally larger than that at the MECP 1. This can be mainly attributed to the greater hopping probability at MECP 2, which is the synergy between the magnitude of gradient difference vector $|\mathbf{x_1}|$ and the SOC . Firstly, no local minimum exists for the ^{1}A state near the ^{3}A stationary point, since once the triplet-to-singlet transition occurs, it goes directly downhill on the singlet PES to form oxirane. On the other hand, there are stationary points on both the ^{3}A$'$ and ^{1}A$''$ states near the MECP 2. Thus, the magnitude of the gradient difference vector $|\mathbf{x_1}|$ is a factor of two larger in the MECP 1 than that in MECP 2. This, along with the slightly larger SOC, makes the hopping probability at MECP 2 roughly two times that of MECP 1.

The unimolecular micro-canonical ISC transition rate constant, $k(E)$, as defined in Equation 3, using both MECPs, are presented in Figure 2(b). It can be noted that $k(E)$ of MECP 2 is 5–7 times that of MECP 1 at collision energy $E > 50$ kcal/mol. This can be traced to the ro-vibrational properties at the two MECPs. In Table 1, it is found that the MECP 1 is essentially in the local region of the ^{3}A stationary point. Thus, the ro-vibrational density of states of MECP 1($\rho_{vr}^{\mathrm{MECP}}$(E)) is fairly consistent with that of ^{3}A stationary point($\rho(E)$). On the contrary, the geometry of MECP 2 is significantly different from that of the ^{3}A$'$ stationary point. This difference in the geometrical and hence ro-vibrational properties makes $k(E)$ at MECP 2 higher.

The canonical transition rate coefficient $k(T)$ is presented in Figure 2(c). There is a striking difference in $k(T)$ calculated using these two MECPs. While the $k(T)$ calculated using MECP 2(solid blue and magenta lines) follows the Arrhenius behavior, that of MECP 1(solid black and read lines) shows negative temperature dependence. To understand this difference, we note that although the potential energy of MECP 1 is slightly higher than that of ^{3}A stationary point, the ZPE corrected activation barrier is -0.90kcal/mol. This effective negative activation energy gives the negative temperature dependence. The ZPE corrected activation energy in MECP 2 is, however, 1.31 kcal/mol, thus, the $k(T)$ follows Arrhenius behavior. To compare our ISC rate coefficient with those used in the literature, we calculate the effective rate coefficient $k_{\mathrm{eff}}(T)$ by thermally averaging the k(T) from the two MECPs according to their relative Boltzmann factors as represented in Figure 2(c) (dashed and solid green lines). Compared to the individual k(T) from the two MECPs, the effective rate constant has weak dependence on the temperature. At room temperature, we found the ISC rate coefficient to be $k_{\mathrm{eff}} = 2.1 \times 10^{12}$ s^{-1}. This number is about an order of magnitude larger than that estimated empirically[1]. In order to verify our results, it would be extremely

beneficial to perform a full master equation calculation using the $k(T)$ used in our study. This is currently under progress.

3. Conclusion

We have probed the unimolecular non-adiabatic ISC in the C_2H_4 O biradical. A four-state description of PES and SOC that governs spin-forbidden transitions are probed using multi-reference electronic structure theories CASSCF and and NEVPT2. Two MECPs between the two pairs of states have been identified. Both the micro-canonical and canonical ISC rate coefficients, obtained from a statistical formulation, predict state-specific energy and temperature-dependenent features. Furthermore, our estimated ISC $k(T)$ is found to be 2.1×10^{12} s^{-1} at room temperature, an order of magnitude larger than that obtained from empirical estimate. Further study is under its way to verify our *ab initio* result.

4. Acknowledgement

This work is supported by the AITSTME project as part of the Predictive Theory and Modeling component of the Materials Genome Initiative. Sandia is a multiprogram laboratory operated by Sandia Corporation, a Lockheed Martin Company, for the National Nuclear Security Administration

[1] T. L. Nguyen, L. Vereecken, X. J. Hou, M. T. Nguyen, J. Peeters, Potential energy surfaces, product distributions and thermal rate coefficients of the reaction of $O(^3P)$ with $C_2H_4(X^1A_g)$: A comprehensive theoretical study, J. Phys. Chem. A 109 (33) (2005) 7489–7499.

[2] J. D. Savee, O. Welz, C. A. Taatjes, D. L. Osborn, New mechanistic insights to the $O(^3P)$ + propene reaction from multiplexed photoionization mass spectrometry, Physical Chemistry Chemical Physics 14 (30) (2012) 10410.

[3] W. Hu, G. Lendvay, B. Maiti, G. C. Schatz, Trajectory surface hopping study of the $O(^3P)$ + ethylene reaction dynamics, J. Phys. Chem. A 112 (10) (2008) 2093–2103.

[4] C. A. Taatjes, D. L. Osborn, T. M. Selby, G. Meloni, A. J. Trevitt, E. Epifanovsky, A. I. Krylov, B. Sirjean, E. Dames, H. Wang, Products of the benzene + $O(^3P)$ reaction, J. Phys. Chem. A 114 (9) (2010) 3355–3370.

[5] T. L. Nguyen, J. Peeters, L. Vereecken, Theoretical reinvestigation of the $O(^3P)$ + C_6H_6 reaction: Quantum chemical and statistical rate calculations, J. Phys. Chem. A 111 (19) (2007) 3836–3849.

[6] B. Fu, Y.-C. Han, J. M. Bowman, L. Angelucci, N. Balucani, F. Leonori, P. Casavecchia, Intersystem crossing and dynamics in $O(^3P)$+C_2H_4 multichannel reaction: Experiment validates theory, Proc. Natl. Acad. Sci. U.S.A. 109 (25) (2012) 97339738.

[7] C. Angeli, R. Cimiraglia, S. Evangelisti, T. Leininger, J.-P. Malrieu, Introduction of n-electron valence states for multireference perturbation theory, J. Chem. Phys. 114 (23) (2001) 10252.

[8] J. C. Lorquet, B. Leyh-Nihant, Nonadiabatic unimolecular reactions. 1. a statistical formulation for the rate constants, J. Phys. Chem. 92 (16) (1988) 47784783.

[9] J. N. Harvey, Understanding the kinetics of spin-forbidden chemical reactions, Phys. Chem. Chem. Phys. 9 (3) (2007) 331.

[10] A. C. West, J. S. Kretchmer, B. Sellner, K. Park, W. L. Hase, H. Lischka, T. L. Windus, $O(^3P)$ + C_2H_4 potential energy surface: Study at the multireference level, J. Phys. Chem. A 113 (45) (2009) 12663–12674.

[11] T. H. Dunning Jr, Gaussian basis sets for use in correlated molecular calculations. I. The atoms boron through neon and hydrogen, J. Chem. Phys. 90 (2) (1989) 1007–1023.

[12] F. Neese, The orca program system, WIREs: Computational Molecular Science 2 (1) (2012) 73–78.

[13] N. Koga, K. Morokuma, Determination of the lowest energy point on the crossing seam between two potential surfaces using the energy gradient, Chem. Phys. Lett. 119 (5) (1985) 371–374.

[14] M. J. Bearpark, M. A. Robb, H. Bernhard Schlegel, A direct method for the location of the lowest energy point on a potential surface crossing, Chem. Phys. Lett. 223 (3) (1994) 269–274.

[15] A. W. Jasper, R. Dawes, Non-born-oppenheimer molecular dynamics of the spin-forbidden reaction $O(^3P) + CO(X^1\Sigma^+) \rightarrow CO2(\tilde{X}^1\Sigma_g^+)$, J. Chem. Phys. 139 (15) (2013) 154313.

[16] C. Zener, Non-adiabatic crossing of energy levels, Proc. R. Soc. A 137 (833) (1932) 696–702.

[17] J. B. Delos, On the reactions of N_2 with O, J. Chem. Phys. 59 (5) (1973) 2365.

Table 1: Properties of MECPs

	CO[a]	CC[b]	dihedral[c]	States[d]	Potential	SO[e]
MECP 1	1.429	1.513	61.5	^{3}A, ^{1}A	0.007[f]	59.1
^{3}A stationary	1.430	1.513	64.3	N/A	0	59.6
MECP 2	1.406	1.529	78.3	^{3}A$'$,^{1}A$''$	3.2[g]	66.5
^{3}A$'$ stationary	1.428	1.524	85.2	N/A	0	66.7

[a] Carbon-Oxygen distance in Å.
[b] Carbon-Carbon distance in Å.
[c] OCCH dihedral in °.
[d] The states that intersect each other.
[e] Spin-orbit coupling in cm^{-1}.
[f] Potential energy relative to the ^{3}A stationary in kcal/mol.
[g] Potential energy relative to the ^{3}A$'$ stationary in kcal/mol.

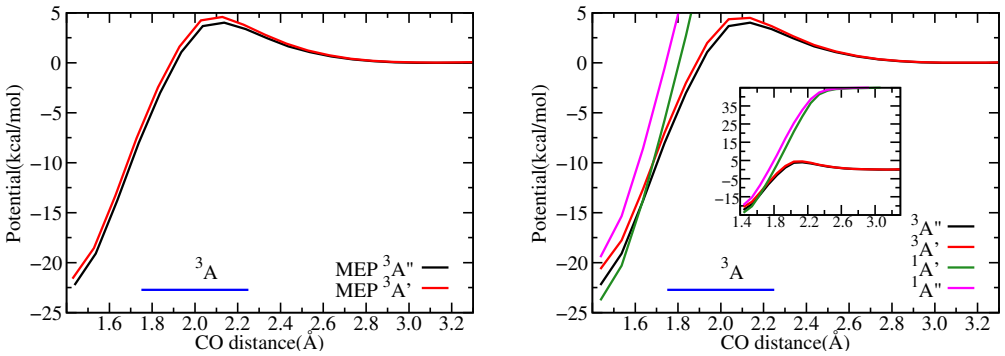

Figure 1: From left to right: (a) the MEP of $^3A''$ and $^3A'$ optimized at the CASSCF level. (b) the energies of the four states, $^3A''$, $^3A'$, $^1A'$ and $^1A''$, calculated using the $^3A''$ MEP geometries. In all cases, the energy is calculated using NEVPT2 theory at the CASSCF optimized geometries.

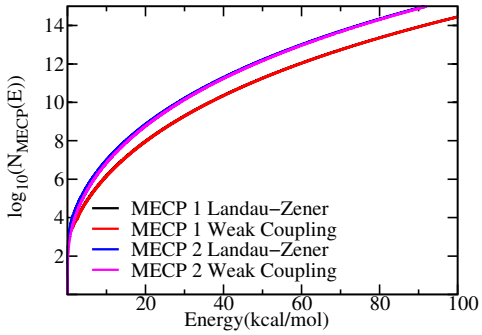

(a)

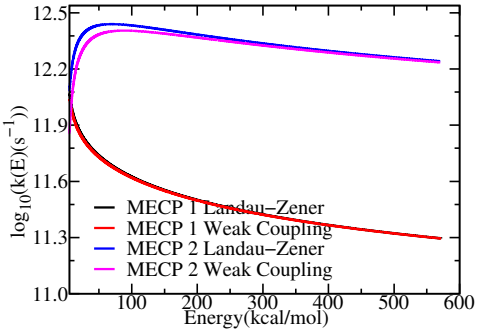

(b)

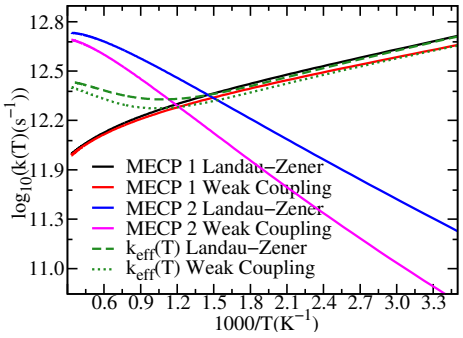

(c)

Figure 2: From top to bottom, (a) the effective number of states, $N_{MECP}(E)$ in Equation 4 (b) the micro-canonical rate constant k(E) in Equation 3 and (c) canonical rate k(T) in Equation 7. In all graphs, results obtained using the hopping probability calculated according to both Landau-Zener and weak coupling formulae are presented . Note that log scale is used for the y axis in all graphs. Results obtained using both MECPs are presented.

Figure 1 From left to right: (a) the MEP of $^3A''$ and $^3A'$ optimized at the CASSCF level. (b) the energies of the four states, $^3A''$, $^3A'$, $^1A'$ and $^1A''$, calculated using the $^3A''$ MEP geometries. In all cases, the energy is calculated using NEVPT2 theory at the CASSCF optimized geometries.

Figure 2 From top to bottom, (a) the effective number of states, $N_{MECP}(E)$ in Equation 4 (b) the micro-canonical rate constant k(E) in Equation 3 and (c) canonical rate k(T) in Equation 7. In all graphs, results obtained using the hopping probability calculated according to both Landau-Zener and weak coupling formulae are presented . Note that log scale is used for the y axis in all graphs. Results obtained using both MECPs are presented.